

## Original Article

# Safety and feasibility of prostatic tissue ablation in dogs by percutaneous irreversible electroporation (IRE) using a newly-developed high-voltage steep-pulse-therapy device

Yu Han<sup>1\*</sup>, Liying Yao<sup>2\*</sup>, Yutang Liu<sup>1</sup>, Haixia Zhang<sup>3</sup>, Zhixiao Xue<sup>1</sup>

<sup>1</sup>Biomedical Engineering and Technology College, Tianjin Medical University, Tianjin 300070, China; <sup>2</sup>Maternity Department, Tianjin Central Obstetrics and Gynecology Hospital, Tianjin 30052, China; <sup>3</sup>Tangshan Vocational Technical College, Hebei 063300, China. \*Equal contributors.

Received January 16, 2019; Accepted May 8, 2019; Epub July 15, 2019; Published July 30, 2019

**Abstract:** Objective: We used a newly-developed high-voltage steep-pulse-therapy device that can generate a microsecond-pulse electrical field to perform irreversible electroporation (IRE) ablation of prostatic tumors. Our aim was to verify the safety and feasibility of prostatic tissue ablation using this high-pressure steep-pulse-therapy device. Methods: Eighteen Beagle dogs underwent real-time ultrasound-guided irreversible electroporation ablation of normal prostate. Two electrode probes were inserted into the prostate tissue under ultrasound guidance with an exposure depth of 1.0 cm and electrode spacing of 1.5 cm. Seventy pulses of 2250 V and a pulse width of 70  $\mu$ s were used for each dog. Hematology, serum biochemistry, histopathology, and ultrastructure were analyzed at 1, 3, 7, 14, and 21 days after IRE ablation. Results: No deaths or serious complications occurred during the experiment. Nanoscale pores appeared on the cell membrane secondary to irreversible electroporation ablation, which resulted in persistent necrosis of prostatic cells. The area of irreversible electroporation ablation was clear, and the urethra and blood vessels were structurally-intact in the ablation area. Conclusions: After irreversible electroporation ablation, the dogs in this model showed prominent ablation effects, and the prostatic architecture was well-preserved. Our results showed that irreversible electroporation ablation of prostatic tissue is safe and feasible using our newly-developed high-voltage steep-pulse-therapy device.

**Keywords:** Irreversible electroporation (IRE), prostate, ultrasound-guided, high-voltage steep-pulse-therapy device

## Introduction

Prostate cancer is the most prevalent cancer among men and the second-leading cause of male cancer-related deaths in the United States. This has resulted in more attention on the diagnosis and treatment of prostate cancer [1]. Surgical resection, radiotherapy, and chemotherapy are the most common methods for treating prostate cancer, but these methods can damage other tissues and cause side effects such as urinary incontinence and erectile dysfunction [2]. Because traditional treatment methods cause appreciable harm to patients' body and mind, patients are more willing to accept minimally-invasive ablation of prostatic tumors, such as cryoablation and ther-

mal ablation; however, these ablation methods also have limitations, and the lack of selectivity may damage the perivascular tumor tissue, urethra, and other important structures [3]. Thermal ablation mainly includes radiofrequency ablation and microwave ablation, but because of the heat-sink effect of the blood vessels, the efficiency of tumor ablation is lower, which results in incomplete ablation [4].

Irreversible electroporation (IRE) is a nonthermal ablation technique that is based on a short-pulse high-voltage electrical field, and is used to create 'nanopores' in the cell membrane, which change cell membrane permeability and lead to cell death [5, 6]. IRE is not temperature-dependent; therefore, IRE is not influenced by

**Table 1.** Main performance of high-pressure steep pulse therapy device

Number of probes	1-6
Number of pulses	1-15
Number of pulse groups	1-250
Pulse amplitude	1000-3000 V
Pulse duration	50 us-100 us
Pulse amplitude accuracy	± 5%
Pulse duration precision	± 2%
Maximum current	50 A

heat-sink. Previous studies have shown that the advantage of IRE is that the technique does not damage important structures in the ablation zone, such as ducts [7], nerves [8], blood vessels [9] and the urethra [2, 10].

The NanoKnife™ system (Angiodynamics, Latham, NY, USA) releases a microsecond-pulsed electrical field between two or more single-stage probes, causing IRE ablation of the tumor. The NanoKnife™ system has been tested in several clinical trials after being approved by the United States Federal Drug Administration in 2012 for clinical trials involving liver cancer [11, 12], pancreatic cancer [13-15], and renal cancer [16, 17].

We systematically studied the safety and feasibility of a newly developed high-voltage steep-pulse-therapy device for ablation of prostatic tissue by evaluating blood examinations, and prostatic tissue histopathology and electron microscopy.

## Materials and methods

### *Experimental device*

The newly developed high-voltage steep-pulse-therapy device (YTL-GM01) used in this study was developed by Tianjin Medical University and Tianjin Intelligent Medical Technology Co., Ltd. The high-voltage steep-pulse-therapy instrument consists of a base, a foot switch, single-electrode probe, an electrocardiograph synchronizer, and a power cord. The high-voltage steep-pulse-therapy device generates a microsecond-pulse electrical field, and the pulse rise time is 200 nanoseconds. The performance indicators of the instrument are shown in **Table 1**.

### *Experimental animals*

Eighteen certified-healthy male Beagle dogs weighing 13-17 kg (housed in the general facilities of Beijing Tonghe Shengtai Institute of Comparative Medicine) were included in this study. The Beijing Tonghe Shengtai Institute of Comparative Medicine was accredited by the Beijing Municipal Science and Technology Commission and carries the Experimental Animal Production License and the Experimental Animal Use License. All animals in the Institute were included and managed in accordance with the requirements of the Guide for Animal Care and Use of Laboratory Animals of our institute. This animal experiment was reviewed and approved by the Animal Experimental Ethics Committee of our institution.

### *IRE ablation procedure*

All 18 Beagle dogs were food-fasted for 24 hours prior to surgery and allowed free access to water. All animals were weighed and then received Xylazine at a dose of 0.1 ml/kg intramuscularly (Jilin Huamao Animal Health Products Co., Ltd., Jilin, china). Preoperatively, we collected 5 ml of venous blood from a forelimb to evaluate each dog's blood and serum biochemistry. After sedation, dogs were placed on the operating table with the inguinal area exposed. The skin of the inguinal area and caudal abdomen was then shaved in an area measuring approximately 6 cm × 3 cm, cleaned, disinfected with iodine, and draped with a surgical drape to isolate the treatment site. IRE was performed using the high-pressure steep-pulse-therapy instrument. Two monopolar probes were inserted in parallel into the prostatic tissue under ultrasound guidance (**Figure 1A** and **1B**). The electrodes had an exposure depth of 1.0 cm and electrode spacing of 1.5 cm. Seventy pulses of 2250 V and a pulse width of 70 μs were used for each dog. Seventeen dogs underwent IRE; one dog did not receive IRE and acted as the control. The control dog was injected intramuscularly with penicillin 800000 IU once daily for 3 days after creating the experimental model.

### *Hematology*

We collected 5 ml of venous blood preoperatively from each dog and marked these as "D0". Three dogs were euthanized on each of day 1,

## Prostatic tissue ablation by irreversible electroporation

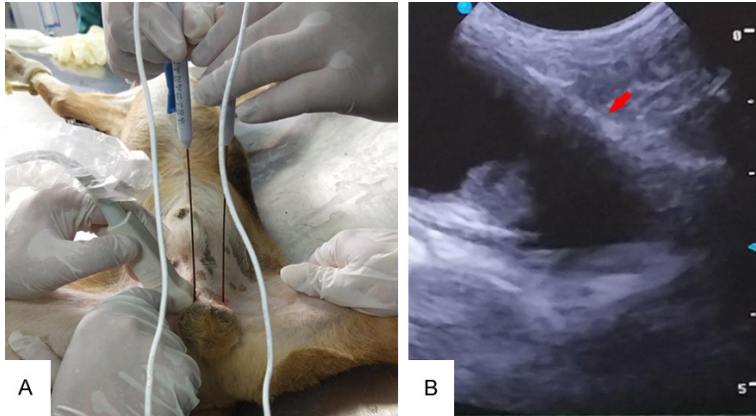


**Figure 1.** IRE ablation of canine prostatic tissue. A. The procedure for IRE ablation of canine prostatic tissue. B. B-ultrasound-guided IRE ablation of prostatic tissue. The red arrow identifies the probe.

**Table 2.** Primer names and associated sequences

Primer Name	Primer Sequence
Caspase3-Forward	5'-TTCATTATTCAGGCCTGCCGAGG-3'
Caspase3-Reverse	5'-TTCTGACAGGCCATGTCATCCTCA-3'

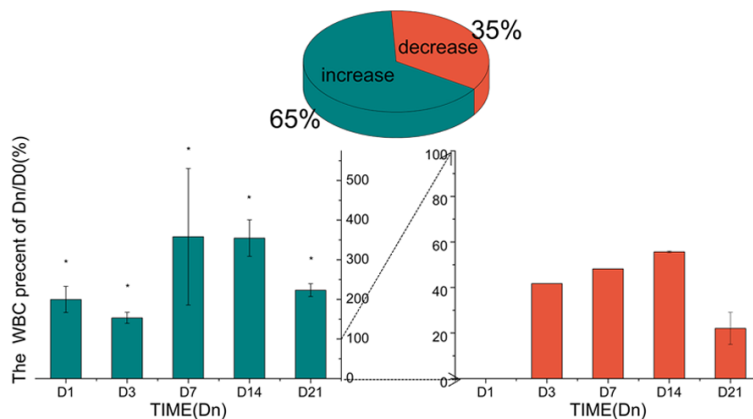


**Figure 2.** Changes in WBC percentage at different time-points. The green bars show the WBC percentage increase at different time-points, and the red bars show the WBC percentage decrease at different time-points. \* $P < 0.05$  versus 100%.

3, and 7 after IRE, and four dogs were euthanized on each of day 14 and 21 after IRE. We collected another 5 mL of venous blood from all dogs before euthanasia and marked these samples as “Dn” ( $n = 1, 3, 7, 14, 21$ ) according to the number of days after IRE. We used a fully-automated hematology analyzer (PE-6800-vet, Shenzhen Pukang Electronics Co., Ltd., Shenzhen, China) to evaluate 20 routine blood values, including white blood cell count (WBC), lymphocyte ratio, granulocytes, and red blood

cell count. We used an automatic biochemical analyzer (SenloSL, Senlong Biological Technology Co., Ltd., Zhuhai, China) to evaluate 31 blood chemistry values, including alanine aminotransferase (ALT), aspartate transaminase (AST), blood urea nitrogen (BUN), and creatinine. Changes in these indicators were compared 1, 3, 7, 14, and 21 days after IRE, and we recorded the percentage as the ratio,  $D_n/D_0$  ( $n = \text{day } 1, 3, 7, 14, \text{ or } 21$ ).

### Gross and histopathological observation

We dissected the prostates in the IRE group after euthanasia on day 1, 3, 7, 14, and 21 after IRE and in the control dogs after euthanasia 7 days after the operation and evaluated the gross and histopathological appearance of the prostatic tissues and IRE-induced wounds. Prostatic ablated and nonablated tissues were collected, and tissues were immersed in 4% paraformaldehyde for 24 hours, then embedded, sectioned, and stained using hematoxylin and eosin for histopathological analysis.

### Ultrastructure observation

The IRE group ablation area and the control dogs' prostatic tissues were collected and fixed in 2.5% glutaraldehyde at 4°C for 2 hours, then evaluated using transmission electron microscopy.

### Reverse transcription polymerase chain reaction

Messenger RNA levels were assessed using quantitative real-time reverse transcription polymerase chain reaction. Total RNA was extracted from prostatic tissues and evaluated using the SimpliNano™ (Biochrom US, Holliston,

## Prostatic tissue ablation by irreversible electroporation

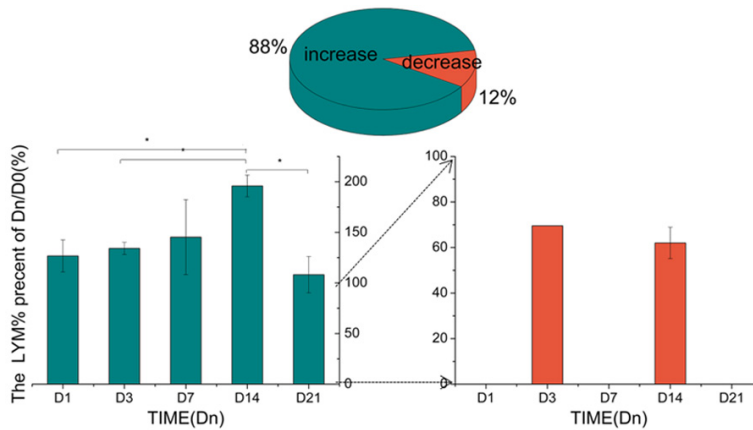


**Figure 3.** Changes in lymphocyte percentage at different time-points. The green bars show the lymphocyte percentage increase at different time-points, and the red bars show the lymphocyte percentage decrease at different time-points. \* $P < 0.05$ .

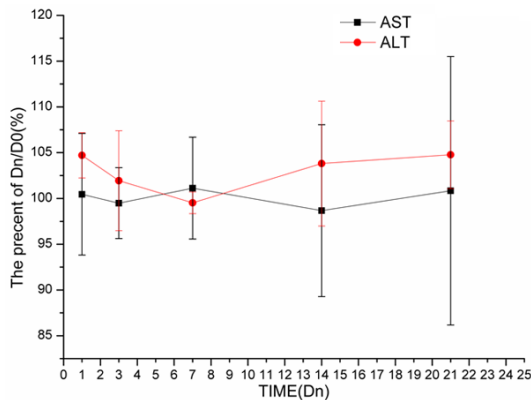


**Figure 4.** Changes in the levels of ALT and AST at difference time-points. Higher than 100% indicates an increase in value, and less than 100% indicates a decrease in value.

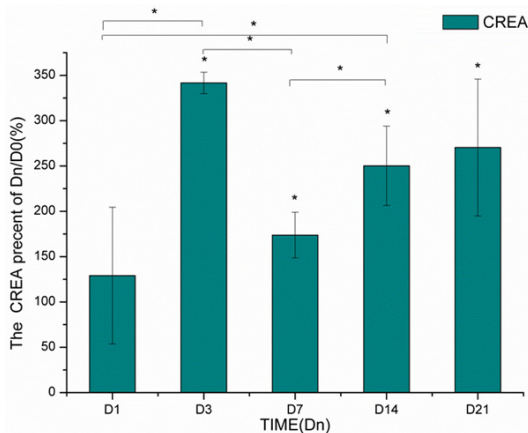


**Figure 5.** Changes in creatinine levels. In the bar chart, higher than 100% indicates an increase in creatinine, and less than 100% indicates a decrease in creatinine. \* $P < 0.05$ .

MA, USA) spectrophotometer for purity and concentration, and RNA was then converted to complementary DNA using the miRNA cDNA Synthesis Kit (ComWin Biotech Co., Ltd, Beijing, China). The sequences for the primers [18] are summarized in supplemental **Table 2**. Results were obtained using the  $\Delta\Delta t$  method.

### Western blot

Protein expression levels of caspase-3 (MDL, Beijing, China) were assessed by Western blot testing. All antibodies were applied according to the manufacturer's instructions. We used the EasySee™ Western Blot Kit (TransGen, Beijing, China) and visualized the protein bands using the Clinx ChemiScope Series Chemiluminescence Imaging systems (Clinx Science Co., Shanghai, China).  $\beta$ -actin protein served as an internal control.

### Statistical analysis

SPSS v.19.0 software was used for statistical analysis (IBM Inc., Armonk, NY, USA). Data were represented as mean  $\pm$  standard deviation. One-way analysis of variance testing was used to assess differences between the two groups, and a one-sample t test was used to assess the difference between each set of data and the defined standard values.  $p < 0.05$  was considered statistically significant.

## Results

### Inflammatory reaction

Compared with preoperative values, WBC increased in 65% of the dogs after IRE and decreased in 35% of the dogs after IRE. The highest percentage WBC was found on day 7 after IRE (D7/D0 = 358%). The D14/D0 WBC ratio was significantly higher compared with D1/D0 ( $p < 0.05$ ); we saw no significant difference between the other ratios ( $p > 0.05$ ) (**Figure 2**). After IRE, 88% of the dogs' lymphocyte ratios were higher than before IRE; 12% of dogs' lymphocyte ratios decreased 3 days and 14 days after IRE, and the lymphocyte ratio

## Prostatic tissue ablation by irreversible electroporation

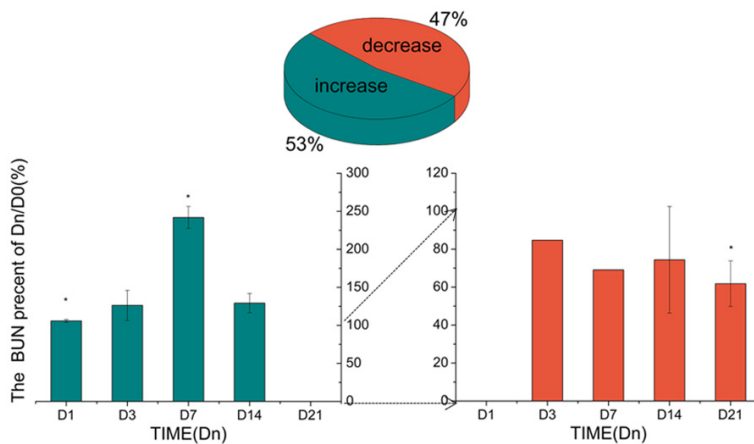


**Figure 6.** Changes in WBC and lymphocyte percentages. The green bars show the percentage increase in lymphocyte ratio at different time-points, and the red bars show the WBC percentage decrease at different time-points. \* $P < 0.05$  versus 100%.

increased the most on day 14 after IRE (D14/D0 = 195.85%). The D14/D0 lymphocyte ratio was significantly higher compared with D1/D0, D3/D0, and D21/D0 ( $p < 0.05$ ). On day 21 after IRE, the lymphocyte ratio recovered to the preoperative level (D21/D0 = 108.13%) (**Figure 3**).

### Liver function

ALT levels on day 1, 3, 7, 14, and 21 after IRE were similar to preoperative values with no significant change ( $P > 0.05$ ). The ALT D7/D0 ratio was significantly lower than the D1/D0 ratio ( $P < 0.05$ ) (**Figure 4**). AST levels on day 1, 3, 7, 14, and 21 after IRE were similar to preoperative values with no significant change ( $P > 0.05$ ) (**Figure 4**).

### Renal function

The creatinine ratio was significantly higher than 100% for D3/D0, D7/D0, D14/D0, and D21/D0 ( $p < 0.05$ ); i.e., creatinine levels were significantly increased on day 3, 7, 14 and 21 after IRE. Creatinine increased most on day 3 after IRE (D3/D0 = 341.67%). The D3/D0 and D14/D0 creatinine ratios were significantly higher than the D1/D0 ratio ( $p < 0.05$ ), and the D7/D0 creatinine ratio was significantly lower than the D3/D0 and D14/D0 ratios ( $p < 0.05$ ) (**Figure 5**).

Fifty-three percent of the dogs had increased BUN on day 1, 3, 7, and 14 after IRE, and 47% of the dogs had decreased BUN on day 3, 7, 14, and 21 after IRE. The BUN ratio was significant-

ly higher than 100% for D1/D0 and D7/D0 ( $p < 0.05$ ), while the D21/D0 BUN ratio was significantly lower than 100% ( $p < 0.05$ ). The BUN ratio increased the most 7 days after IRE (D7/D0 = 241.91%), and the BUN ratio decreased the most 21 days after IRE (D21/D0 = 61.80%) (**Figure 6**).

### Gross observation and histopathological observation

No dogs died, and we encountered no serious complications during the study. All dogs' attitude, behavioral activity, and feed intake returned to normal after IRE. One day

after IRE, the perforation site was firm, and the perforation wound was partially infected, but the urethra was undamaged. Three days after IRE, the wound became more diffuse and dark purple in color. On day 8 after IRE, wound tissue damage was evident, the perforation distance had decreased, and the prostatic tissue had atrophied. On days 14 and 21 after IRE, the outer membrane of the prostate was thinned and the internal tissues were clearly visible (**Figure 7A**). Histopathological results showed that the prostatic vesicles in the control dog were tightly-arranged and full of glandular cavities. In IRE dogs, hemorrhage was severe in the prostatic ablation area on day 1 and 3 after IRE, and no bleeding was observed in the surrounding prostatic tissue. On days 7, 14, and 21 after IRE, hemorrhage had decreased, and glandular atrophy was found in both the ablated area and the surrounding area. In addition, atrophy of the glandular cavity was more severe in the ablated area than in the surrounding area (**Figure 7B**). After IRE, the urethral mucosa was damaged and ruptured, but the muscle layer and connective tissue was unaffected (**Figure 7C, 7D**).

### Ultrastructural observation

On day 1 after IRE, the number of mitochondria decreased markedly, cells were shrunken and cell volume decreased, cell space widened and gap contents decreased, cytoplasmic color lightened, and there were flecks in some cell cytoplasm. On day 3 after IRE, the mitochondria were larger and darker in color, with less cytoplasm and no obvious intercellular bound-

Prostatic tissue ablation by irreversible electroporation

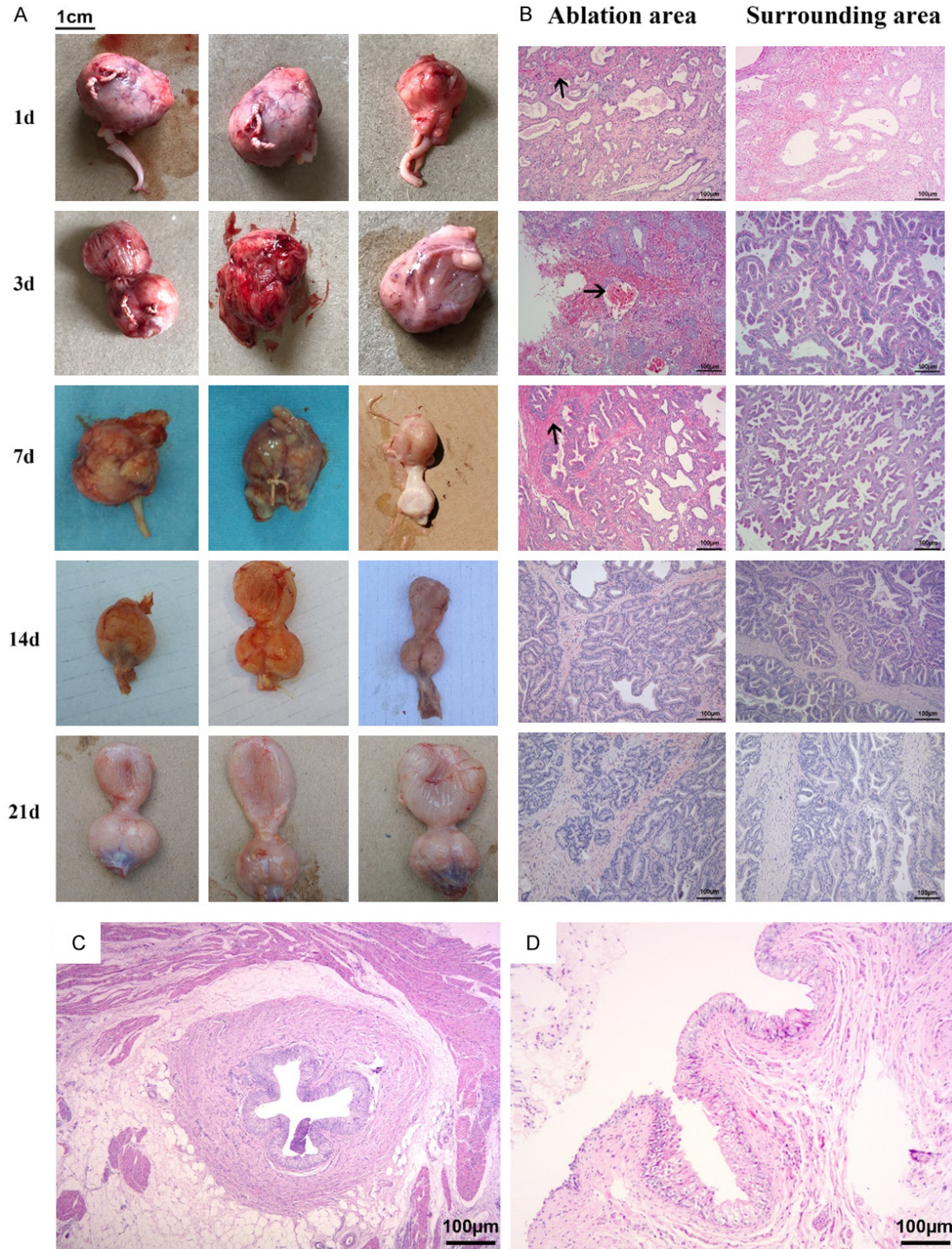


**Figure 7.** Gross and histopathological findings. A. Photograph of prostatic tissue at different time-points. B. Hematoxylin and eosin staining of the ablated area and surrounding area in the prostatic tissue at different time-points. The black arrows indicate hemorrhagic reaction. C. Hematoxylin and eosin staining of a cross-section of the urethra (magnification,  $\times 400$ ). D. Histological staining of the longitudinal urethra (magnification,  $\times 400$ ).

ary. On day 7 after IRE, many large vacuoles appeared, and the cell outlines were blurred. There were large numbers of vacuoles on day

14 after IRE; the amount of cytoplasm had decreased more than the previous days, and the nuclear chromosomes were aggregated. On

## Prostatic tissue ablation by irreversible electroporation

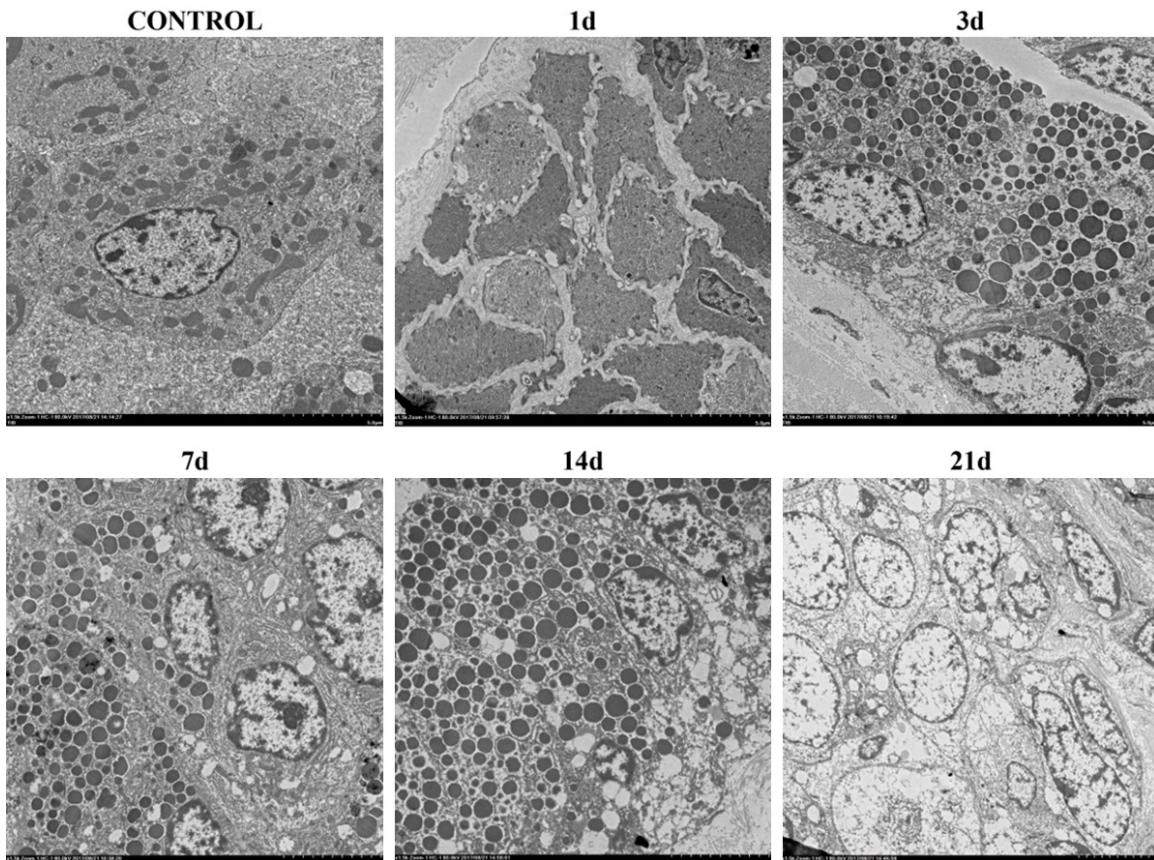


**Figure 8.** Ultrastructural changes in prostatic tissue post-IRE at different time-points. Changes in the cell ultrastructure are seen (magnification,  $\times 1500$ ).

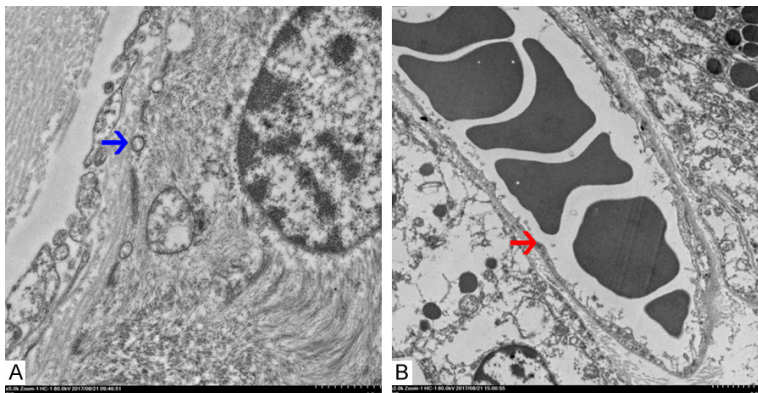


**Figure 9.** Observation of cell membranes and blood vessels by transmission electron microscopy. A. Nanopores on the cell membrane (magnification,  $\times 5000$ ) (blue arrow). B. Blood vessel (magnification,  $\times 2000$ ) (red arrow).

day 21 after IRE, the mitochondria had disappeared, and there was almost no cytoplasm; only a small amount of rough endoplasmic reticulum and vacuoles could be seen in the cells (**Figure 8**).

One day after IRE, many small pores appeared on the cell membrane, and the cell membrane became discontinuous (**Figure 9A**). No blood vessel epidermal cells were observed after IRE, but the vascular structure remained intact (**Figure 9B**).

### *Expression of caspase3*

We evaluated the expression of caspase-3 at different times after IRE, and found that expression of caspase-3 was highest on day 3 after IRE.

Caspase-3 expression on day 3 and 7 was significantly higher than that on day 1 after IRE. Caspase-3 expression on day 21 after IRE was significantly lower than that on day 1 after IRE (**Figure 10A-C**).

## Prostatic tissue ablation by irreversible electroporation

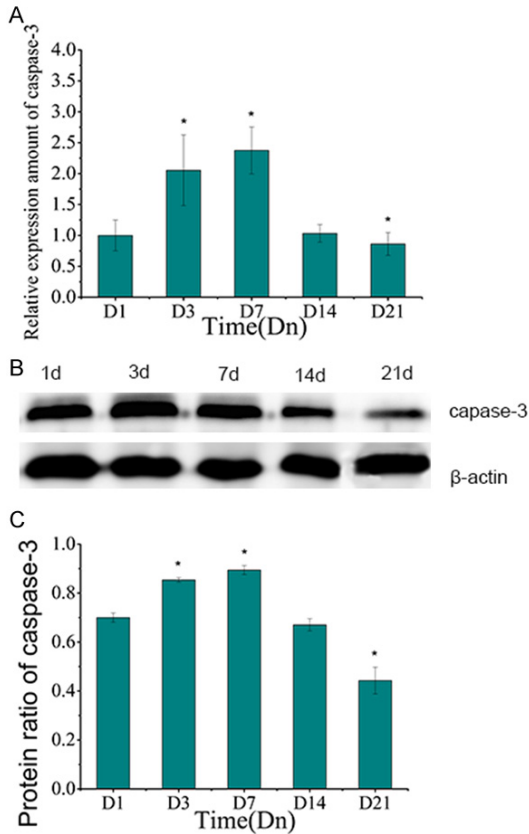


**Figure 10.** Expression of caspase-3 at difference time-points. A. Relative expression of caspase-3 at different time-points after IRE. B. Protein expression of caspase-3 and actin. C. Relative gray-scale analysis of caspase-3. \* $P < 0.05$  versus D1 values.

### Discussion

In this study, we used a Beagle model to systematically study the safety and feasibility of IRE ablation of the prostate gland by performing blood examinations, and evaluating the appearance, pathology, and ultrastructure of the prostate. Onik et al. [7] performed IRE ablation on the prostate tissues of six male dogs and encountered no deaths, behavioral abnormalities, or serious complications after surgery; our results were similar.

Luo et al. [19] found that after IRE ablates the tumor, WBC and lymphocyte counts increased on day 7 after IRE but then gradually decreased. Li et al. [20] reported that WBC levels gradually increased within 1 day after IRE and gradually decreased thereafter until returning to normal levels on day 7. In our study, WBC levels increased most significantly on day 7 after IRE,

and then began to decrease gradually, but remained higher than preoperative levels. The lymphocyte ratio increased the most on day 14 after IRE, reaching preoperative levels by day 21 post-IRE. Our results showed that dogs can develop inflammation after IRE ablation of prostatic tissue, however, within 14 days after IRE, inflammation gradually decreased.

When IRE ablates liver tumors, a rapid rise in alkaline phosphatase and AST is seen within 1 day after IRE, which is a sign of liver cell injury or necrosis [21]. When IRE was used to ablate the pancreas, Anabel et al. [22] found that ALT and AST were elevated 6 hours after IRE and returned to normal 1 day after IRE. We began measurements on day 1 after IRE, and found that ALT and AST changed very little and remained similar to preoperative levels, suggesting that IRE ablation of prostatic tissue has almost no effect on liver function and does not damage the liver. In contrast, both creatinine and BUN levels increased significantly after IRE ablation of prostatic tissue, indicating kidney damage [23]. In addition, decreased BUN has also been seen in some animals and may also indicate kidney disease [24].

The ultrastructural observation of IRE-ablated tissue revealed that prostatic cells did not immediately die, but instead, underwent a slow, persistent death, and complete cell death was seen on day 14. Histopathology also revealed tissue necrosis within the ablated area on days 14 and 21, confirming that IRE effectively kills prostatic cells.

Caspase-3 is the most important terminal cleavage enzyme during apoptosis. After IRE, the amount of caspase-3 protein increased, leading to apoptosis of prostatic cells. On day 14 after IRE, ablated prostatic tissue was mostly necrotic, and apoptosis was less visible.

The electrical field formed by the needle electrode in IRE devices is extremely uneven, and the electrical field intensity in the area around the needle electrode is the largest, with the electrical field intensity gradually decreasing as the distance between the ablation area and the electrode needle increases [25]. Because of the heterogeneity of IRE ablation, when a tumor is ablated, tissue further away from the acupuncture point may not be ablated, which is the main reason that ablation does not completely

destroy tumors [26]. Several researchers are studying this issue, mainly through the optimization of treatment options, to ensure complete tumor ablation [27]. Obtaining clear IRE ablation boundaries with a transition between the ablated and nonablated areas of only a few cells will help researchers design new treatment options.

Transmission electron micrographs revealed that after IRE ablation, the cell membrane was destroyed, and multiple nanopores appeared. Nanopores change cell permeability, which destroys the cell's internal environment, resulting in cell death [2]. IRE ablation does not damage blood vessels within the ablation zone, although we saw almost no vascular epithelial cells in ablated prostatic tissue using electron microscopy. However, the vascular structure remained intact because blood vessels are rich in elastic fibers, and IRE does not damage elastic fibers. When IRE is used to treat prostatic cancer, the presence of blood vessels increases the potential for prostatic tissue regeneration; however, tissue regeneration after tumor destruction is not a concern [7]. We saw no signs of tissue regeneration in this study, probably because the follow-up time was too short, and further studies with longer duration are required.

The prostatic urethra contains an epithelial layer, fibrous layer, and muscular layer. Urethral disease is generally caused by the loss of the full-thickness urethra [28]. Onlik et al. [7] studied IRE ablation of dog prostatic tissue and found no damage to the urethra. However, in our study, IRE damaged the epithelial layers of the prostatic urethra while leaving the fibrous layer undamaged, which is beneficial to urethral recovery.

In this study, we successfully performed IRE ablation of the canine prostate, which caused slow, persistent death of prostatic tissue. In addition, IRE ablation did not damage the overall structure of the blood vessels and urethra, and no serious complications occurred. Our experimental results showed that it was safe and feasible to use our newly-developed high-voltage steep-pulse-therapy device to perform IRE ablation of canine prostatic tissue.

### Acknowledgements

This work was supported by the Tianjin Science and Technology Committee (14CDZSY00037).

We thank Jane Charbonneau, DVM, from Liwen Bianji, Edanz Group China ([www.liwenbianji.cn/ac](http://www.liwenbianji.cn/ac)), for editing the English text of a draft of this manuscript.

### Disclosure of conflict of interest

None.

**Address correspondence to:** Zhixiao Xue, Biomedical Engineering and Technology College, Tianjin Medical University, Tianjin 300070, China. Tel: 13821074-823; E-mail: [xuezhixiao@126.com](mailto:xuezhixiao@126.com)

### References

- [1] Yao C, Dong S, Zhao Y, Lv Y, Liu H, Gong L, Ma J, Wang H and Sun Y. Bipolar microsecond pulses and insulated needle electrodes for reducing muscle contractions during irreversible electroporation. *IEEE Trans Biomed Eng* 2017; 64: 2924-2937.
- [2] Valerio M, Dickinson L, Ali A, Ramachandran N, Donaldson I, Freeman A, Ahmed HU and Emberton M. A prospective development study investigating focal irreversible electroporation in men with localised prostate cancer: nanoknife electroporation ablation trial (NEAT). *Contemp Clin Trials* 2014; 39: 57-65.
- [3] Jourabchi N, Beroukheim K, Tafti BA, Kee ST and Lee EW. Irreversible electroporation (NanoKnife) in cancer treatment. *Gastrointestinal Intervention* 2014; 3: 8-18.
- [4] Wagstaff PG, Buijs M, van den Bos W, de Bruin DM, Zondervan PJ, de la Rosette JJ and Laguna Pes MP. Irreversible electroporation: state of the art. *Onco Targets Ther* 2016; 9: 2437-2446.
- [5] Al-Sakere B, Andre F, Bernat C, Connault E, Opolon P, Davalos RV, Rubinsky B and Mir LM. Tumor ablation with irreversible electroporation. *PLoS One* 2007; 2: e1135.
- [6] Wagstaff PG, de Bruin DM, Zondervan PJ, Savci Heijink CD, Engelbrecht MR, van Delden OM, van Leeuwen TG, Wijkstra H, de la Rosette JJ and Laguna Pes MP. The efficacy and safety of irreversible electroporation for the ablation of renal masses: a prospective, human, in-vivo study protocol. *BMC Cancer* 2015; 15: 165.
- [7] Choi JW, Lu DS, Osuagwu F, Raman S and Lassman C. Assessment of chronological effects of irreversible electroporation on hilar bile ducts in a porcine model. *Cardiovasc Intervent Radiol* 2014; 37: 224-230.
- [8] Schoellnast H, Monette S, Ezell PC, Deodhar A, Maybody M, Erinjeri JP, Stubblefield MD, Single GW Jr, Hamilton WC Jr, Solomon SB. Acute and subacute effects of irreversible electroporation on nerves: experimental study in a pig model. *Radiology* 2011; 260: 421-427.

## Prostatic tissue ablation by irreversible electroporation

- [9] Chen X, Ren Z, Zhu T, Zhang X, Peng Z, Xie H, Zhou L, Yin S, Sun J and Zheng S. Electric Ablation with irreversible electroporation (IRE) in vital hepatic structures and follow-up investigation. *Sci Rep* 2015; 5: 16233.
- [10] Neal RE 2nd, Millar JL, Kavnoudias H, Royce P, Rosenfeldt F, Pham A, Smith R, Davalos RV and Thomson KR. In vivo characterization and numerical simulation of prostate properties for non-thermal irreversible electroporation ablation. *Prostate* 2014; 74: 458-468.
- [11] Dollinger M, Beyer LP, Haimerl M, Niessen C, Jung EM, Zeman F, Stroszczynski C and Wiggermann P. Adverse effects of irreversible electroporation of malignant liver tumors under CT fluoroscopic guidance: a single-center experience. *Diagn Interv Radiol* 2015; 21: 471-475.
- [12] Dollinger M, Zeman F, Niessen C, Lang SA, Beyer LP, Muller M, Stroszczynski C and Wiggermann P. Bile duct injury after irreversible electroporation of hepatic malignancies: evaluation of MR imaging findings and laboratory values. *J Vasc Interv Radiol* 2016; 27: 96-103.
- [13] Orcutt S, Kis B and Malafa M. Case report: Irreversible electroporation for locally advanced pancreatic cancer. *Int J Surg Case Rep* 2017; 40: 54-57.
- [14] Hitchcock KE, Nichols RC, Morris CG, Bose D, Hughes SJ, Stauffer JA, Celinski SA, Johnson EA, Zaiden RA, Mendenhall NP and Rutenberg MS. Feasibility of pancreatotomy following high-dose proton therapy for unresectable pancreatic cancer. *World J Gastrointest Surg* 2017; 9: 103-108.
- [15] Scheffer HJ, Vroomen LG, de Jong MC, Melendorst MC, Zonderhuis BM, Daams F, Vogel JA, Besselink MG, van Kuijk C, Witvliet J, de van der Schueren MA, de Gruijl TD, Stam AG, van den Tol PM, van Delft F, Kazemier G and Meijerink MR. Ablation of locally advanced pancreatic cancer with percutaneous irreversible electroporation: results of the phase I/II PAN-FIRE study. *Radiology* 2017; 282: 585-597.
- [16] Thomson KR, Cheung W, Ellis SJ, Federman D, Kavnoudias H, Loader-Oliver D, Roberts S, Evans P, Ball C and Haydon A. Investigation of the safety of irreversible electroporation in humans. *J Vasc Interv Radiol* 2011; 22: 611-621.
- [17] Pech M, Janitzky A, Wendler JJ, Strang C, Blaschke S, Dudeck O, Ricke J and Liehr UB. Irreversible electroporation of renal cell carcinoma: a first-in-man phase I clinical study. *Cardiovasc Intervent Radiol* 2011; 34: 132-138.
- [18] Zhou P, Tu L, Lin X, Hao X, Zheng Q, Zeng W, Zhang X, Zheng Y, Wang L and Li S. cfa-miR-143 promotes apoptosis via the p53 pathway in canine influenza virus H3N2-infected cells. *Viruses* 2017; 9: 360.
- [19] Luo X, Qin Z, Tao H, Shi J, Fang G, Li Z, Zhou X, Chen J, Xu K, Zeng J and Niu L. The safety of irreversible electroporation on nerves adjacent to treated tumors. *World Neurosurg* 2017; 108: 642-649.
- [20] Li J, Zeng J, Chen J, Shi J, Luo X, Fang G, Chai W, Zhang W, Liu T and Niu L. Evaluation of the safety of irreversible electroporation on the stomach wall using a pig model. *Exp Ther Med* 2017; 14: 696-702.
- [21] Tian G, Zhao Q, Chen F, Jiang T and Wang W. Ablation of hepatic malignant tumors with irreversible electroporation: a systematic review and meta-analysis of outcomes. *Oncotarget* 2017; 8: 5853-5860.
- [22] Jose A, Sobrevals L, Ivorra A and Fillat C. Irreversible electroporation shows efficacy against pancreatic carcinoma without systemic toxicity in mouse models. *Cancer Lett* 2012; 317: 16-23.
- [23] Jae-Chen S, Young-Joo J, Seon-Min P, Kang Seok S, Jung-Hyun S and Jung-II C. Mechanism underlying renal failure caused by pathogenic *Candida albicans* infection. *Biomed Rep* 2015; 3: 179-182.
- [24] Manickam C, Wachtman L, Martinot AJ, Giavedoni LD and Reeves RK. Metabolic dysregulation in hepatitis B infection of common marmosets (*Callithrix jacchus*). *PLoS One* 2017; 12: e0170240.
- [25] Garcia PA, Davalos RV and Miklavcic D. A numerical investigation of the electric and thermal cell kill distributions in electroporation-based therapies in tissue. *PLoS One* 2014; 9: e103083.
- [26] Wendler JJ, Ricke J, Pech M, Fischbach F, Jurgens J, Siedentopf S, Roessner A, Porsch M, Baumunk D, Schostak M, Kollermann J and Liehr UB. First delayed resection findings after irreversible electroporation (IRE) of human localized renal cell carcinoma (RCC) in the IRENE pilot phase 2a trial. *Cardiovasc Intervent Radiol* 2016; 39: 239-250.
- [27] Edd JF and Davalos RV. Mathematical modeling of irreversible electroporation for treatment planning. *Technol Cancer Res Treat* 2007; 6: 275-286.
- [28] Zhou S, Yang R, Zou Q, Zhang K, Yin T, Zhao W, Shapter JG, Gao G and Fu Q. Fabrication of tissue-engineered bionic urethra using cell sheet technology and labeling by ultrasmall superparamagnetic iron oxide for full-thickness urethral reconstruction. *Theranostics* 2017; 7: 2509-2523.